An International Journal of Computational Thermal Sciences, vol. 1, pp. xx–xx, 2009

HIGHER-ORDER SPHERICAL HARMONICS TO MODEL RADIATION IN DIRECT NUMERICAL SIMULATION OF TURBULENT REACTING FLOWS

Kshitij V. Deshmukh, Michael F. Modest and Daniel C. Haworth

Department of Mechanical and Nuclear Engineering, The Pennsylvania State University, University Park, PA, USA

The exact treatment of the radiative transfer equation (RTE) is difficult even for idealized situations and simple boundary conditions. A number of higher-order approximations, such as the moment method, discrete ordinates method and spherical harmonics method, provide efficient solution methods. A statistical method, such as the photon Monte Carlo method, solves the RTE by simulating radiative processes such as emission, absorption, and scattering. Although accurate, it requires large computational resources and the solution suffers from statistical noise. The third-order spherical harmonics method (P_3 approximation) used here decomposes the RTE into a set of 16 first-order partial differential equations. Successive elimination of spherical harmonic tensors reduces this set to six coupled second-order partial differential equations with general boundary conditions, allowing for variable properties and arbitrary three-dimensional geometries. The tedious algebra required to assemble the final form is offset by greater accuracy because it is a spectral method as opposed to the finite difference/finite volume approach of the discrete ordinates method. The radiative solution is coupled with a direct numerical solution (DNS) of turbulent reacting flows to isolate and quantify turbulence–radiation interactions. These interactions arise due to nonlinear coupling between the fluctuations of temperature, species concentrations, and radiative intensity. Radiation properties employed here correspond to a nonscattering fictitious gray gas with a Planck-mean absorption coefficient, which mimics that of typical hydrocarbon-air combustion products. Individual contributions of emission and absorption TRI have been isolated and quantified. The temperature self-correlation, the absorption coefficient–Planck function correlation, and the absorption coefficient–intensity correlation have been examined for small to large values of the optical thickness. Contributions from temperature self-correlation and absorption coefficient–Planck function correlation have been found to be significant for all the three optical thicknesses while absorption coefficient–intensity correlation is significant for optically thick cases, weak for optically intermediate cases, and negligible for optically thin cases.

Correspondence concerning this article should be addressed to Michael F. Modest, Department of Mechanical and Nuclear Engineering, The Pennsylvania State University, University Park, PA, USA; e-mail:mfmodest@psu.edu.

ISSN 1940-2503/09/35.00

INTRODUCTION

Most practical combustion devices involve turbulent fluid flow, and the high temperatures prevalent in most combustion processes result in substantial heat transfer by radiation. An accurate description of turbulence and combustion by themselves is mathematically complex and computationally expensive. This has often resulted in the neglect of radiation in turbulent combustion applications, or its treatment using simple models, to avoid the additional complexity of solving the radiative transfer equation (RTE) (Modest, 2003).

The RTE is an integrodifferential equation consisting of up to five independent variables (three in space and two in direction). An exact analytical solution to the RTE can be obtained only for a few simple situations, such as one-dimensional (1D) plane-parallel media without scattering. On the other hand, accurate numerical solutions for practical scenarios are exceedingly difficult to obtain. In addition, for typical combustion gases, such as carbon dioxide and water vapor, the strong spectral variation in radiative properties demands large computational resources for line-by-line spectral calculations. A number of approximate methods have been developed over time, which simplify computation and have reasonable accuracy. Among these approximate methods the spherical harmonics method (SHM), the discrete ordinates method (DOM) or the finite volume method, (FVM) the zonal method and the photon Monte Carlo method (PMC) have been used most frequently (Modest, 2003). The zonal method was popular in the past decades due to its simplicity. But its solution requires inversion of full matrices and the method becomes computationally very expensive for complex problems and for optically thick media. In addition, it cannot treat anisotropic scattering. The DOM/FVM method approximates the directional variation of the radiative intensity rather than its spatial behavior. It employs a discrete representation of the directional variation with integrals over the total solid angle 4π obtained via numerical quadrature. It is relatively simple to implement but has several drawbacks. For a scattering medium and/or reflecting walls, the DOM/FVM method requires an iterative solution. In addition, its convergence is known to slow down for optically thick media. Furthermore, the DOM may suffer ray effects and possibly false scattering due to its angular discretization (Chai et al., 1993).

The spherical harmonics method (SHM) also approximates the directional variation of the radiative intensity like the DOM, but here the directional distribution of intensity is expressed as a series of spherical harmonics. The SPH method converts the integrodifferential RTE into relatively simple partial differential equations, similar to the DOM/FVM; however, unlike the DOM/FVM these can be solved using standard PDE solver packages. In this method, the spatial and directional dependencies are completely decoupled, allowing independent choices for spatial and directional accuracy without suffering detrimental ray effects. The lowest-order P_N approximation, the P_1 approximation, has enjoyed great popularity because of its relative simplicity and compatibility with standard methods for the solution of the energy equation (Modest, 2003). However,

the P_1 approximation performs poorly in the optically thin limit and other strongly non-isotropic radiative intensity fields. Mathematical complexity increases rapidly if higher-order P_N approximations for multidimensional geometry are desired, which is probably responsible for the fact that its development lags behind that for the DOM/FVM. The fact that in the SHM intensity is expressed in terms of spherical harmonics makes it difficult to accurately represent directionally strongly anisotropic intensity as encountered, for example, near emitting walls and/or in optically thin media. This can be largely mitigated by using the modified differential approximation approach of Olfe (1967) and Modest (1989).

A number of higher-order P_N approximations have been formulated for specific (usually 1D) geometries (Kofink, 1959; Bayazitoğlu and Higenyi, 1979; Tong and Swathi, 1987; Ratzel and Howell, 1983; Mengüç and Viskanta, 1985) and for limited three-dimensional (3D) applications (Davison, 1958; Ou and Liou, 1982), as recently reviewed by Yang and Modest (2007). Yang and Modest developed a successive elimination methodology, which decomposes the RTE into $N(N+1)/2$ coupled, second-order, elliptic partial differential equations for a given odd order N, allowing for variable properties and arbitrary three-dimensional geometries.

Even when radiation was considered, the traditional approach of modeling radiative transfer in combustion chambers has largely ignored turbulence–radiation interactions (TRI). In turbulent combustion scenarios, turbulence, combustion, and radiation are tightly coupled processes and the physics of one affects the other two. The interaction between turbulence and radiation is a two-way process. The turbulent fluctuations affect radiation fluxes and radiation may, in turn, modify turbulent fluctuations. At first, only radiative properties evaluated based on mean quantities were considered (Grosshandler and Sawyer, 1977; Viskanta and Mengüç, 1987) used an exponential wide-band spectral model in addition to mean properties to predict spectral radiative intensities in fires. Wilcox (1975) used an exponential wideband spectral model in addition to mean properties to predict spectral radiative intensities in fires. Tamanini (1977) studied round turbulent flames assuming the emission to be proportional to the local reaction rate and thereby taking flame radiation as a fixed fraction of the chemical energy release. The measured mean flame properties by Grosshandler and Sawyer (1977) were used to study spectral radiation properties for methane/air combustion products. Souil et al. (1984) studied radiation from turbulent diffusion flames to vertical target surfaces using mean temperature values.

However, the nonlinear dependence of radiation on temperature coupled with the fluctuations in temperature (encountered in turbulent configurations) tend to enhance radiative transfer. The experimental and numerical work of (Faeth et al., 1985; Gore and Faeth, 1986, 1988; Gore et al., 1987; Kounalakis et al., 1988, 1989, 1991) demonstrated that radiative emission from, both, luminous and nonluminous turbulent flames may be as much as 300% higher than the value expected based on mean values of temperature and

absorption coefficient. This was generally assumed to be predominantly due to the nonlinear dependence of radiation on temperature. This evidence of the effect of turbulence on radiation was supported by early simplified numerical studies, in which the radiation calculations were not coupled with turbulence calculations. The expansion of emissive power into a Taylor series was employed by Cox (1977) to show that flame emission increases by a large amount with an increase in temperature fluctuations. Nelson (1989) concluded that turbulence−radiation interactions were dominated by temperature fluctuations when studying band radiation from a fluctuating medium. The study of gas radiation from a homogeneous turbulent medium by Kritzstein and Soufiani (1993) concluded that radiative intensities increase with increase in temperature fluctuations, while concentration fluctuations had only a weak effect on radiative intensities. Soufiani et al. (1990a, 1990b) investigated nonlinear effects of radiation in a channel flow of a nonreacting radiating gas. In this study, the mean radiative wall flux predicted with and without considering the nonlinear effects of radiation was different by only 10%: the absence of combustion results in smaller turbulent fluctuations as compared to those produced in the presence of combustion, resulting in a weak TRI. Song and Viskanta (1987) studied turbulent flames inside a two-dimensional furnace by solving the fully coupled reacting flow and radiation problem with simplifying assumptions, such as the use of a presumed PDF for mixture fraction and heat release rate. They found increases in radiative fluxes of up to 80% due to temperature and concentration field fluctuations in cases where the flame occupied a large fraction of the furnace volume. Their approach was extended by Hartick et al. (1996) to a diffusion flame. Krebs et al. (1996) applied a Reynolds averaging method to the radiative transfer equation and showed that emission from radiation increases more at shorter wavelengths due to scalar fluctuations.

All these treatments to study effects of turbulence on radiation were of an approximate nature as no knowledge of the fluctuations in temperature and concentration fields was available (i.e., an assumption for the PDF or a simplification regarding the turbulence was necessary). More recently, Mazumder and Modest (1990a) introduced a direct PDF method and applied it to a methane-air diffusion flame in a bluff body combustor by solving the velocity-composition PDF equation using a Monte Carlo method. The thin eddy approximation (Kabashinikov and Myasnikova, 1985) was invoked to study turbulence-radiation interactions. The inclusion of the absorption coefficient-temperature correlation alone was found to increase radiative heat flux by 40-45% (Mazumder and Modest, 1990b). Li and Modest (2003) used a composition PDF method to investigate the importance of turbulence-radiation interactions and the important correlations that need to be considered in simulations. They found that the absorption coefficient-Planck function correlation is important in addition to the temperature self-correlation. Coelho (2004) reported a nearly 50% increase in radiative heat loss due to TRI for a nonpremixed methane-air turbulent jet flame, while Tessé et al. (2004) reported a 30% increase in radiative heat loss with consideration of TRI for a sooty, nonpremixed ethylene-air tur-

bulent jet flame. Wu et al. (2005, 2007) were the first to study TRI for an idealized turbulent premixed flame using direct numerical simulation (DNS) coupled with a photon Monte Carlo method for the solution of the RTE; they found that emission and absorption are both enhanced when TRI are considered, and that both effects remained important even at relatively low optical thicknesses. Recently, Deshmukh et al. (2007) studied TRI using DNS for a canonical configuration of homogeneous isotropic turbulence for a nonpremixed system. In their study, the interaction of turbulence and radiative intensity resulted in substantial emission and absorption TRI.

Here, DNS coupled with a third-order SHM (P_3 approximation) is used to isolate and quantify TRI effects in a statistically one-dimensional premixed system. The aims are to provide new fundamental physical insight into TRI in chemically reacting turbulent flows and to provide guidance for model development. The details of P_3 approximation are provided next, followed by the equation set for turbulent premixed combustion scenario, the nature of turbulence-radiation interactions and the description of the model problem. Results and a discussion are provided after the description of the model problem.

P_3 APPROXIMATION

The general form of the RTE is given (Modest, 2003) as

$$\hat{s} \cdot \nabla_\tau I + I = (1 - \omega) I_b + \frac{\omega}{4\pi} \int_{4\pi} I(\hat{s}') \Phi(\hat{s} \cdot \hat{s}') d\Omega' \tag{1}$$

where ω is the single scattering albedo. Augmentation of intensity due to in-scattering is calculated by the last term in Eq. (1), where Φ is the scattering phase function and describes the probability that a ray from direction $\hat{s}'$ will be scattered into a certain direction, $\hat{s}$. The intensity gradient, ∇_τ, along direction $\hat{s}$ is written in terms of nondimensional optical coordinates with the extinction coefficient β and $d\tau = \beta ds$.

The radiative intensity field $I(\mathbf{r}, \hat{s})$ at a point $\mathbf{r}$ can be thought to be a surface of a unit sphere surrounding the point $\mathbf{r}$. Such a function may be expressed as a 2D generalized Fourier series,

$$I(\mathbf{r}, \hat{s}) = \sum_{n=0}^{\infty} \sum_{m=-n}^{n} I_n^m(\mathbf{r}) Y_n^m(\hat{s}) \tag{2}$$

where the $I_n^m(\mathbf{r})$ are position dependent coefficients and the $Y_n^m(\hat{s})$ are *spherical harmonics*, given by

$$Y_n^m(\hat{s}) = \begin{cases} \cos(m\phi) P_n^m(\cos\theta), & \text{for} \quad m \geq 0 \\ \sin(|m|\phi) P_n^m(\cos\theta), & \text{for} \quad m < 0 \end{cases} \tag{3}$$

Here, θ and ϕ are the polar and azimuthal angles defining the direction of the unit vector $\hat{s}$ and $P_n^m(\cos\theta)$ are *associated Legendre polynomials* given by

$$P_n^m(\mu) = (-1)^m \frac{(1-\mu^2)^{|m|/2}}{2^n n!} \frac{d^{n+|m|}}{d^{n+|m|}\mu}(\mu^2-1)^n \tag{4}$$

The P_3 approximation is obtained by substituting a truncated the Fourier series of Eq. (2) at $n = 3$ in Eq. (1). The highest value for n retained gives the method its order and name. After tedious algebra, it results in a set of $(3+1)^2 = 16$ first-order partial differential equations. Yang and Modest (2007) employed successive elimination of spherical harmonic tensors to reduce the set to $3(3+1)/2 = 6$ second-order elliptic partial differential equations. The set for Cartesian geometry is given below

$$\begin{aligned}
&\frac{\partial}{\partial\tau_x}\left[2\gamma_{8,3}\frac{\partial I_2^{-2}}{\partial\tau_x} - \gamma_{1,1}\frac{\partial I_2^0}{\partial\tau_y} + 2\gamma_{7,-3}\frac{\partial I_2^2}{\partial\tau_y} + \gamma_{2,-3}\frac{\partial I_2^{-1}}{\partial\tau_z} + \frac{5}{\alpha_1}\frac{\partial I_0}{\partial\tau_y}\right] \\
&+\frac{\partial}{\partial\tau_y}\left[2\gamma_{8,3}\frac{\partial I_2^{-2}}{\partial\tau_y} - \gamma_{1,1}\frac{\partial I_2^0}{\partial\tau_x} - 2\gamma_{7,-3}\frac{\partial I_2^2}{\partial\tau_x} + \gamma_{2,-3}\frac{\partial I_2^1}{\partial\tau_z} + \frac{5}{\alpha_1}\frac{\partial I_0}{\partial\tau_x}\right] \\
&+\frac{\partial}{\partial\tau_z}\left[\frac{10}{\alpha_3}\frac{\partial I_2^{-2}}{\partial\tau_z} - \frac{5}{\alpha_3}\frac{\partial I_2^1}{\partial\tau_y} - \frac{5}{\alpha_3}\frac{\partial I_2^{-1}}{\partial\tau_x}\right] - 2\alpha_2 I_2^{-2} = 0, \quad \text{for} \quad Y_2^{-2}
\end{aligned} \tag{5a}$$

$$\begin{aligned}
&\frac{\partial}{\partial\tau_x}\left[\gamma_{6,1}\frac{\partial I_2^0}{\partial\tau_x} + 3\gamma_{-4,1}\frac{\partial I_2^1}{\partial\tau_z} - 6\gamma_{1,1}\frac{\partial I_2^2}{\partial\tau_x} - 6\gamma_{1,1}\frac{\partial I_2^{-2}}{\partial\tau_y} - \frac{5}{\alpha_1}\frac{\partial I_0}{\partial\tau_x}\right] \\
&+\frac{\partial}{\partial\tau_y}\left[\gamma_{6,1}\frac{\partial I_2^0}{\partial\tau_y} + 3\gamma_{-4,1}\frac{\partial I_2^{-1}}{\partial\tau_z} + 6\gamma_{1,1}\frac{\partial I_2^2}{\partial\tau_y} - 6\gamma_{1,1}\frac{\partial I_2^{-2}}{\partial\tau_x} - \frac{5}{\alpha_1}\frac{\partial I_0}{\partial\tau_y}\right] \\
&+\frac{\partial}{\partial\tau_z}\left[\gamma_{9,4}\frac{\partial I_2^0}{\partial\tau_z} + 3\gamma_{3,-2}\frac{\partial I_2^1}{\partial\tau_x} + 3\gamma_{3,-2}\frac{\partial I_2^{-1}}{\partial\tau_y} + \frac{10}{\alpha_1}\frac{\partial I_0}{\partial\tau_z}\right] - \alpha_2 I_2^0 = 0, \text{ for } Y_2^0
\end{aligned} \tag{5b}$$

$$\begin{aligned}
&\frac{\partial}{\partial\tau_x}\left[2\gamma_{8,3}\frac{\partial I_2^2}{\partial\tau_x} - \gamma_{1,1}\frac{\partial I_2^0}{\partial\tau_x} - 2\gamma_{7,-3}\frac{\partial I_2^{-2}}{\partial\tau_y} + \frac{5}{\alpha_1}\frac{\partial I_0}{\partial\tau_x} + \gamma_{2,-3}\frac{\partial I_2^1}{\partial\tau_z}\right] \\
&+\frac{\partial}{\partial\tau_y}\left[2\gamma_{8,3}\frac{\partial I_2^2}{\partial\tau_y} + \gamma_{1,1}\frac{\partial I_2^0}{\partial\tau_y} + 2\gamma_{7,-3}\frac{\partial I_2^{-2}}{\partial\tau_x} - \frac{5}{\alpha_1}\frac{\partial I_0}{\partial\tau_y} - \gamma_{2,-3}\frac{\partial I_2^{-1}}{\partial\tau_z}\right] \\
&+\frac{\partial}{\partial\tau_z}\left[\frac{10}{\alpha_3}\frac{\partial I_2^2}{\partial\tau_z} - \frac{5}{\alpha_3}\frac{\partial I_2^1}{\partial\tau_x} + \frac{5}{\alpha_3}\frac{\partial I_2^{-1}}{\partial\tau_y}\right] - 2\alpha_2 I_2^2 = 0, \quad \text{for} \quad Y_2^2
\end{aligned} \tag{5c}$$

$$\frac{\partial}{\partial\tau_x}\left[\frac{5}{\alpha_1}\frac{\partial I_0}{\partial\tau_x}-\frac{1}{\alpha_1}\frac{\partial I_2^0}{\partial\tau_x}+\frac{6}{\alpha_1}\frac{\partial I_2^2}{\partial\tau_x}+\frac{6}{\alpha_1}\frac{\partial I_2^{-2}}{\partial\tau_y}-\frac{3}{\alpha_1}\frac{\partial I_2^1}{\partial\tau_z}\right]$$
$$+\frac{\partial}{\partial\tau_y}\left[\frac{5}{\alpha_1}\frac{\partial I_0}{\partial\tau_y}-\frac{1}{\alpha_1}\frac{\partial I_2^0}{\partial\tau_y}-\frac{6}{\alpha_1}\frac{\partial I_2^2}{\partial\tau_y}+\frac{6}{\alpha_1}\frac{\partial I_2^{-2}}{\partial\tau_x}-\frac{3}{\alpha_1}\frac{\partial I_2^{-1}}{\partial\tau_z}\right]$$
$$+\frac{\partial}{\partial\tau_z}\left[\frac{5}{\alpha_1}\frac{\partial I_0}{\partial\tau_z}+\frac{2}{\alpha_1}\frac{\partial I_2^0}{\partial\tau_z}-\frac{3}{\alpha_1}\frac{\partial I_2^1}{\partial\tau_x}-\frac{3}{\alpha_1}\frac{\partial I_2^{-1}}{\partial\tau_y}\right]=5\alpha_0\left(I_0-4\pi I_b\right),\ \text{for } Y_0 \tag{5d}$$

$$\frac{\partial}{\partial\tau_x}\left[-\frac{10}{\alpha_3}\frac{\partial I_2^{-2}}{\partial\tau_z}+\frac{5}{\alpha_3}\frac{\partial I_2^1}{\partial\tau_y}+\frac{5}{\alpha_3}\frac{\partial I_2^{-1}}{\partial\tau_x}\right]$$
$$+\frac{\partial}{\partial\tau_y}\left[\gamma_{8,3}\frac{\partial I_2^{-1}}{\partial\tau_y}+\gamma_{3,-2}\frac{\partial I_2^0}{\partial\tau_z}-\gamma_{2,-3}\frac{\partial I_2^1}{\partial\tau_x}+\frac{10}{\alpha_3}\frac{\partial I_2^2}{\partial\tau_z}-\frac{5}{\alpha_1}\frac{\partial I_0}{\partial\tau_z}\right]$$
$$+\frac{\partial}{\partial\tau_z}\left[\gamma_{8,3}\frac{\partial I_2^{-1}}{\partial\tau_z}+\gamma_{-4,1}\frac{\partial I_2^0}{\partial\tau_y}-2\gamma_{2,-3}\frac{\partial I_2^2}{\partial\tau_y}+2\gamma_{2,-3}\frac{\partial I_2^{-2}}{\partial\tau_x}-\frac{5}{\alpha_1}\frac{\partial I_0}{\partial\tau_y}\right]$$
$$-\alpha_2 I_2^{-1}=0,\quad \text{for}\quad Y_2^{-1} \tag{5e}$$

$$\frac{\partial}{\partial\tau_x}\left[\gamma_{8,3}\frac{\partial I_2^1}{\partial\tau_x}+\gamma_{3,-2}\frac{\partial I_2^0}{\partial\tau_z}-\gamma_{2,-3}\frac{\partial I_2^{-1}}{\partial\tau_y}-\frac{10}{\alpha_3}\frac{\partial I_2^2}{\partial\tau_z}-\frac{5}{\alpha_1}\frac{\partial I_0}{\partial\tau_z}\right]$$
$$+\frac{\partial}{\partial\tau_y}\left[-\frac{10}{\alpha_3}\frac{\partial I_2^{-2}}{\partial\tau_z}+\frac{5}{\alpha_3}\frac{\partial I_2^1}{\partial\tau_y}+\frac{5}{\alpha_3}\frac{\partial I_2^{-1}}{\partial\tau_x}\right]$$
$$+\frac{\partial}{\partial\tau_z}\left[\gamma_{8,3}\frac{\partial I_2^1}{\partial\tau_z}+\gamma_{-4,1}\frac{\partial I_2^0}{\partial\tau_x}+2\gamma_{2,-3}\frac{\partial I_2^2}{\partial\tau_x}+2\gamma_{2,-3}\frac{\partial I_2^{-2}}{\partial\tau_y}-\frac{5}{\alpha_1}\frac{\partial I_0}{\partial\tau_x}\right]$$
$$-\alpha_2 I_2^1=0,\quad \text{for}\quad Y_2^1 \tag{5f}$$

where

$$\gamma_{i,j}=\left(\frac{i}{\alpha_3}+\frac{j}{\alpha_1}\right) \tag{6}$$

and

$$\alpha_n=(2n+1)-\omega A_n \tag{7}$$

A_n is a coefficient for higher-order approximation of anisotropic scattering.

Because the intensity is expressed as a truncated series, the boundary conditions are satisfied approximately by minimizing the difference between the intensity predicted by P_3 approximation, $I(\mathbf{r},\hat{s})$ and the actual surface intensity, $I_s(\mathbf{r}_w,\hat{s})$ at the boundary. Marshak's boundary conditions (Marshak, 1947), which minimize this difference in an integral sense were chosen by Yang and Modest (2007) as they appear to be flexible and accurate. Their general form can be given as

$$\int_{\hat{n}\cdot\hat{s}>0} I(\tau_w,\hat{s})\bar{Y}^m_{2i-1}d\Omega = \int_{\hat{n}\cdot\hat{s}>0} I_s(\tau_w,\hat{s})\bar{Y}^m_{2i-1}d\Omega \qquad (8)$$
$$i = 1,2,...,\frac{1}{2}(N+1), \text{all relevant } m$$

where the $\bar{Y}$ denote spherical harmonics measured from a local spherical coordinate system, with polar angle $\bar{\theta}$ measured from the surface normal (local $\bar{z}$-axis), and $\bar{\phi}$ in the plane of the surface (measured from a local $\bar{x}$-axis). "All relevant m" implies choosing a set consistent with the P_N-approximation. For example, for the P_3 approximation six boundary conditions are needed: $i = 1$ provides three ($m = -1, 0, +1$), and another three must come from $i = 2$ [usually chosen as the smallest m-values (i.e., $m = -1, 0, +1$)]. After extremely tedious algebra, where the global spherical harmonics are rotated into the local coordinate system, the boundary conditions are obtained as below.

For the x direction [the upper sign in $(\pm)$ and $(\mp)$ applies to $x = 0$ and the lower one to $x = L$],

$$\bar{Y}_1^{-1}: -\frac{3}{4}I_2^1 \pm \frac{6}{5\alpha_1}\frac{\partial I_2^1}{\partial\tau_x} \mp \frac{6}{5\alpha_1}\frac{\partial I_2^{-1}}{\partial\tau_y} \pm \frac{2}{5\alpha_1}\frac{\partial}{\partial\tau_z}\left[5I_0 + 2I_2^0\right] = 0 \qquad (9a)$$

$$\bar{Y}_1^0: I_0 - \frac{1}{8}I_2^0 + \frac{3}{4}I_2^2 \mp \frac{2}{5\alpha_1}\frac{\partial}{\partial\tau_x}\left[5I_0 - I_2^0 + 6I_2^2\right] \pm \frac{12}{5\alpha_1}\frac{\partial I_2^{-2}}{\partial\tau_y} \mp \frac{6}{5\alpha_1}\frac{\partial I_2^1}{\partial\tau_z} = 4\pi I_s \qquad (9b)$$

$$\bar{Y}_1^1: \frac{3}{2}I_2^{-2} \mp \frac{12}{5\alpha_1}\frac{\partial I_2^{-2}}{\partial\tau_x} \pm \frac{2}{5\alpha_1}\frac{\partial}{\partial\tau_y}\left[5I_0 - I_2^0 - 6I_2^2\right] \mp \frac{6}{5\alpha_1}\frac{\partial I_2^{-1}}{\partial\tau_z} = 0 \qquad (9c)$$

$$\bar{Y}_3^{-2}: I_2^{-1} \mp \frac{16}{5\alpha_3}\frac{\partial I_2^{-1}}{\partial\tau_x} \pm \frac{16}{5\alpha_3}\frac{\partial I_2^1}{\partial\tau_y} \mp \frac{32}{5\alpha_3}\frac{\partial I_2^{-2}}{\partial\tau_z} = 0 \qquad (9d)$$

$$\bar{Y}_3^0: I_0 + \frac{1}{2}I_2^0 - 3I_2^2 \mp \frac{24}{5\alpha_3}\frac{\partial}{\partial\tau_x}\left[\frac{1}{2}I_2^0 - 3I_2^2\right] \pm \frac{48}{5\alpha_3}\frac{\partial I_2^{-2}}{\partial\tau_y} \mp \frac{24}{5\alpha_3}\frac{\partial I_2^1}{\partial\tau_z} = 4\pi I_s \qquad (9e)$$

$$\bar{Y}_3^2: \frac{1}{4}I_2^0 + \frac{1}{2}I_2^2 \mp \frac{16}{5\alpha_3}\frac{\partial}{\partial\tau_x}\left[\frac{1}{4}I_2^0 + \frac{1}{2}I_2^2\right] \mp \frac{16}{5\alpha_3}\frac{\partial I_2^{-2}}{\partial\tau_y} \mp \frac{8}{5\alpha_3}\frac{\partial I_2^1}{\partial\tau_z} = 0 \qquad (9f)$$

For the y direction [the upper sign in $(\pm)$ and $(\mp)$ applies to $y = 0$ and the lower one to $y = L$],

$$\bar{Y}_1^{-1}: \frac{3}{4}I_2^{-1} \mp \frac{6}{5\alpha_1}\frac{\partial I_2^1}{\partial \tau_x} \mp \frac{6}{5\alpha_1}\frac{\partial I_2^{-1}}{\partial \tau_y} \mp \frac{2}{5\alpha_1}\frac{\partial}{\partial \tau_z}\left[5I_0 + 2I_2^0\right] = 0 \tag{10a}$$

$$\bar{Y}_1^{0}: I_0 - \frac{1}{8}I_2^0 - \frac{3}{4}I_2^2 \mp \frac{12}{5\alpha_1}\frac{\partial I_2^{-2}}{\partial \tau_x} \mp \frac{2}{5\alpha_1}\frac{\partial}{\partial \tau_y}\left[5I_0 - I_2^0 - 6I_2^2\right] \mp \frac{6}{5\alpha_1}\frac{\partial I_2^{-1}}{\partial \tau_z} = 4\pi I_s \tag{10b}$$

$$\bar{Y}_1^{1}: -\frac{3}{2}I_2^{-2} \pm \frac{2}{5\alpha_1}\frac{\partial}{\partial \tau_x}\left[5I_0 - I_2^0 + 6I_2^2\right] \pm \frac{12}{5\alpha_1}\frac{\partial I_2^{-2}}{\partial \tau_y} \pm \frac{6}{5\alpha_1}\frac{\partial I_2^{1}}{\partial \tau_z} = 0 \tag{10c}$$

$$\bar{Y}_3^{-2}: I_2^1 \mp \frac{16}{5\alpha_3}\frac{\partial I_2^{-1}}{\partial \tau_x} \mp \frac{16}{5\alpha_3}\frac{\partial I_2^{1}}{\partial \tau_y} \mp \frac{32}{5\alpha_3}\frac{\partial I_2^{-2}}{\partial \tau_z} = 0 \tag{10d}$$

$$\bar{Y}_3^{0}: I_0 + \frac{1}{2}I_2^0 + 3I_2^2 \mp \frac{48}{5\alpha_3}\frac{\partial I_2^{-2}}{\partial \tau_x} \mp \frac{24}{5\alpha_3}\frac{\partial}{\partial \tau_y}\left[\frac{1}{2}I_2^0 + 3I_2^2\right] \mp \frac{24}{5\alpha_3}\frac{\partial I_2^{-1}}{\partial \tau_z} = 4\pi I_s \tag{10e}$$

$$\bar{Y}_3^{2}: -\frac{1}{4}I_2^0 + \frac{1}{2}I_2^2 \mp \frac{16}{5\alpha_3}\frac{\partial I_2^{-2}}{\partial \tau_x} \mp \frac{16}{5\alpha_3}\frac{\partial}{\partial \tau_y}\left[-\frac{1}{4}I_2^0 + \frac{1}{2}I_2^2\right] \pm \frac{8}{5\alpha_3}\frac{\partial I_2^{-1}}{\partial \tau_z} = 0 \tag{10f}$$

For the z direction [the upper sign in $(\pm)$ and $(\mp)$ applies to $z = 0$ and the lower one to $z = L$],

$$\bar{Y}_1^{-1}: \frac{3}{4}I_2^{-1} \pm \frac{12}{5\alpha_1}\frac{\partial I_2^{-2}}{\partial \tau_x} \pm \frac{2}{5\alpha_1}\frac{\partial}{\partial \tau_y}\left[5I_0 - I_2^0 - 6I_2^2\right] \mp \frac{6}{5\alpha_1}\frac{\partial I_2^{-1}}{\partial \tau_z} = 0 \tag{11a}$$

$$\bar{Y}_1^{0}: I_0 + \frac{1}{4}I_2^0 \pm \frac{6}{5\alpha_1}\frac{\partial I_2^{1}}{\partial \tau_x} \pm \frac{6}{5\alpha_1}\frac{\partial I_2^{-1}}{\partial \tau_y} \mp \frac{2}{5\alpha_1}\frac{\partial}{\partial \tau_z}\left[5I_0 + 2I_2^0\right] = 4\pi I_s \tag{11b}$$

$$\bar{Y}_1^{1}: \frac{3}{4}I_2^{1} \pm \frac{2}{5\alpha_1}\frac{\partial}{\partial \tau_x}\left[5I_0 - I_2^0 + 6I_2^2\right] \pm \frac{12}{5\alpha_1}\frac{\partial I_2^{-2}}{\partial \tau_y} \mp \frac{6}{5\alpha_1}\frac{\partial I_2^{1}}{\partial \tau_z} = 0 \tag{11c}$$

$$\bar{Y}_3^{-2}: I_2^{-2} \pm \frac{8}{5\alpha_3}\frac{\partial I_2^{-1}}{\partial \tau_x} \mp \frac{16}{5\alpha_3}\frac{\partial I_2^{1}}{\partial \tau_y} \pm \frac{8}{5\alpha_3}\frac{\partial I_2^{-2}}{\partial \tau_z} = 0 \tag{11d}$$

$$\bar{Y}_3^{0}: I_0 - I_2^0 \pm \frac{24}{5\alpha_3}\frac{\partial I_2^{1}}{\partial \tau_x} \pm \frac{24}{5\alpha_3}\frac{\partial I_2^{-1}}{\partial \tau_y} \pm \frac{24}{5\alpha_3}\frac{\partial I_2^{0}}{\partial \tau_z} = 4\pi I_s \tag{11e}$$

$$\bar{Y}_3^{2}: I_2^{2} \pm \frac{8}{5\alpha_3}\frac{\partial I_2^{1}}{\partial \tau_x} \mp \frac{8}{5\alpha_3}\frac{\partial I_2^{-1}}{\partial \tau_y} \mp \frac{16}{5\alpha_3}\frac{\partial I_2^{2}}{\partial \tau_z} = 0 \tag{11f}$$

CONSERVATION EQUATIONS

The three main computational approaches for simulating turbulent reacting flows are Reynolds averaged Navier-Stokes system (RANS), large eddy simulation (LES), and direct numerical simulation. Here, direct numerical simulation is used. The set of equations solved for compressible turbulent flows comprises conservation of mass, linear momentum, and energy. In Cartesian tensor notation,

$$\frac{\partial \rho}{\partial t} + \frac{\partial \rho u_i}{\partial x_i} = 0 \tag{12}$$

$$\frac{\partial \rho u_i}{\partial t} + \frac{\partial \rho u_i u_j}{\partial x_j} = -\frac{\partial p}{\partial x_i} + \frac{\partial \tau_{ij}}{\partial x_j} \tag{13}$$

$$\frac{\partial \rho E}{\partial t} + \frac{\partial (\rho E + p) u_i}{\partial x_i} = \frac{\partial u_j \tau_{ij}}{\partial x_i} + \frac{\partial}{\partial x_i}\left(\lambda \frac{\partial T}{\partial x_i}\right) + Q\dot{\omega}_T - \nabla \cdot \vec{q}_{\text{rad}} \tag{14}$$

where λ is thermal conductivity, Q is the heat release of the reaction per unit mass of reactants, $\dot{\omega}_T$ is the reaction rate, $\nabla \cdot \vec{q}_{\text{rad}}$ is the radiative source term, and

$$\rho E = \frac{1}{2}(\rho u_k u_k) + \frac{p}{\gamma - 1} \tag{15}$$

is the total internal energy, using the ideal gas law,

$$p = \rho R T \tag{16}$$

Finally,

$$\tau_{ij} = \mu \left(\frac{\partial u_i}{\partial x_j} + \frac{\partial u_j}{\partial x_i} - \frac{2}{3}\delta_{ij} \frac{\partial u_k}{\partial x_k} \right) \tag{17}$$

is the stress vector.

This set of equations is sufficient to solve for a nonreacting turbulent flow field if boundary and initial conditions are specified. This involves solving for five quantities called primitive variables. These are density, ρ, the three velocity components in the three directions of the Cartesian coordinate system, u_i, and one variable for energy, E (or pressure, p, or enthalpy, or temperature, T). Additional equations are needed to solve for variables introduced by considering chemical and radiative effects. The species of combustion are characterized through their mass fractions Y_k for $k = 1, 2, ..., N$, where N is the number of species in the reacting mixture ($N = 3$ in the present study). The mass fractions Y_k are defined by

$$Y_k = \frac{m_k}{m} \tag{18}$$

where m_k is the mass of species k in a given volume and m is the total mass of the volume.

The number of variables that describe chemically reacting turbulent flows is $N + 5$ instead of 5 as in the case of nonreacting turbulent flows. Thus, N additional equations need to be introduced, one for each species. This implies that the computing effort required to solve chemically reacting turbulent flows will be many times greater than that of nonreacting turbulent flows if the number of species is large.

Using Fick's law for diffusion, the species transport equation for any species k is given as

$$\frac{\partial \rho Y_k}{\partial t} + \frac{\partial (\rho Y_k u_i)}{\partial x_i} = \frac{\partial}{\partial x_i}\left(\rho \mathcal{D}_k \frac{\partial Y_k}{\partial x_i}\right) - \dot{\omega}_k, \qquad k = 1, 2, \ldots, N \tag{19}$$

where $\mathcal{D}_k$ is the diffusion coefficient and $\dot{\omega}_k$ is the species reaction rate. Additionally, for the study under consideration, the molecular transport coefficients (viscosity μ, thermal conductivity λ, and species diffusion $\mathcal{D}_k$) depend on temperature in such a way that the Prandtl number, Pr, and Schmidt numbers, Sc_k, are constant. As a consequence, the Lewis numbers, Le_k, is a constant as well,

$$\lambda = \mu \frac{c_p}{\mathrm{Pr}}, \qquad \mathcal{D}_k = \frac{\mu}{\rho \mathrm{Sc}_k}, \qquad \mathrm{Le}_k = \frac{\mathrm{Sc}_k}{\mathrm{Pr}} \tag{20}$$

Additional details can be found in Haworth and Poinsot (1996).

TURBULENCE RADIATION INTERACTIONS IN CHEMICALLY REACTING FLOWS

The radiation source term in the instantaneous energy equation can be expressed as the divergence of the radiative heat flux $\vec{q}_{\mathrm{rad}}$. For the special case of a gray nonscattering medium,

$$\nabla \cdot \vec{q}_{\mathrm{rad}} = 4\kappa_P \sigma T^4 - \kappa_P G \tag{21}$$

where κ_P is the Planck-mean absorption coefficient (Modest, 2003), σ is the Stefan-Boltzmann constant and G the direction-integrated incident radiation [I_0 in Eq. (5d)]. The first term on the right-hand side of Eq. (21) corresponds to emission and the second to absorption. TRI is brought into evidence by taking the mean of Eq. (21)

$$\langle \nabla \cdot \vec{q}_{\mathrm{rad}} \rangle = 4\sigma \langle \kappa_P T^4 \rangle - \langle \kappa_P G \rangle \tag{22}$$

where angled brackets denote mean quantities.

In the emission term, TRI appears as the correlation between the Planck-mean absorption coefficient and the fourth power of temperature (the spectrally integrated Planck function, I_b): $\langle \kappa_P T^4 \rangle = \langle \kappa_P \rangle \langle T^4 \rangle + \langle \kappa_P' \cdot (T^4)' \rangle$, where a prime denotes a fluctuation about the local mean. Emission TRI can be decomposed into the temperature self-correlation $\left(\langle T^4 \rangle \neq \langle T \rangle^4\right)$ and the absorption coefficient–Planck function correlation.

In the absorption term, TRI appears as the correlation between the absorption coefficient and the intensity (or incident radiation), $\langle \kappa_P G \rangle = \langle \kappa_P \rangle \langle G \rangle + \langle \kappa'_P G' \rangle$.

In the present study, we explore TRI in a statistically one-dimensional, nonstationary, turbulent, nonpremixed system using DNS. The principal quantities examined are the normalized means $\mathcal{R}_{T^4}$, $\mathcal{R}_{\kappa I_b}$, and $\mathcal{R}_{\kappa G}$,

$$\mathcal{R}_{T^4} \equiv \frac{\langle T^4 \rangle}{\langle T \rangle^4} \, , \; \mathcal{R}_{\kappa I_b} \equiv \frac{\langle \kappa'_P I'_b \rangle}{\langle \kappa_P \rangle \langle I_b \rangle} \, , \; \mathcal{R}_{\kappa G} \equiv \frac{\langle \kappa'_P G' \rangle}{\langle \kappa_P \rangle \langle G \rangle} \tag{23}$$

In the absence of TRI, $\mathcal{R}_{T^4}$ would be equal to unity, and $\mathcal{R}_{\kappa I_b}$, and $\mathcal{R}_{\kappa G}$ would each be equal to zero. The departures of each quantity from these values allow different contributions to TRI to be isolated and quantified.

A dimensionless optical thickness κL is introduced, where L is an appropriate length scale. Kabashnikov and Kmit (1979), Kabashnikov (1985), Kabashnikov and Myasnikova (1985) suggested that, if the mean free path for radiation is much larger than the turbulence eddy length scale, then the fluctuations in κ (a quantity dependent on local properties) should be uncorrelated with those in G (a nonlocal quantity), so that $\langle \kappa G \rangle \approx \langle \kappa \rangle \langle G \rangle$: this is the "optically thin fluctuation approximation" (OTFA) ($\kappa L \ll 1$). At the other extreme ($\kappa L \gg 1$), the optical thickness may be large compared to all hydrodynamic and chemical scales. In that case, fluctuations in intensity are generated locally and would be expected to be correlated strongly with those of the absorption coefficient: a diffusion approximation is appropriate in that case (Modest, 2003). Between these extremes are cases where the smallest scales (Kolmogorov microscales and/or flame thickness) are optically thin while the largest (integral scales) are optically thick. Modeling of such intermediate cases is an outstanding challenge in TRI and is the primary motivation for this study.

STATISTICALLY ONE-DIMENSIONAL PREMIXED FLAME

Computational Configuration

A statistically one-dimensional, transient, turbulent premixed system is considered as shown in Fig. 1 with premixed reactants (blue) entering from the negative x-direction and hot products (red) leaving from the positive x-direction. A laminar premixed flame is superposed on a 3D homogeneous turbulent field. The configuration is a cube of sides 1.44 with 144 grid nodes in the y- and z-directions and 145 grid nodes in the x-direction. The boundaries are periodic in the y- and z-directions. The extra grid node in the x-direction is due to the nonperiodic boundaries, which are nonreflecting (Poinsot and Lele, 1992). For radiation, the x-direction inlet boundary is considered cold: radiation incident on this boundary is absorbed and no emission occurs at the boundary while the outlet boundary is considered hot: the boundary is treated as a black surface at the exit fluid temperature.

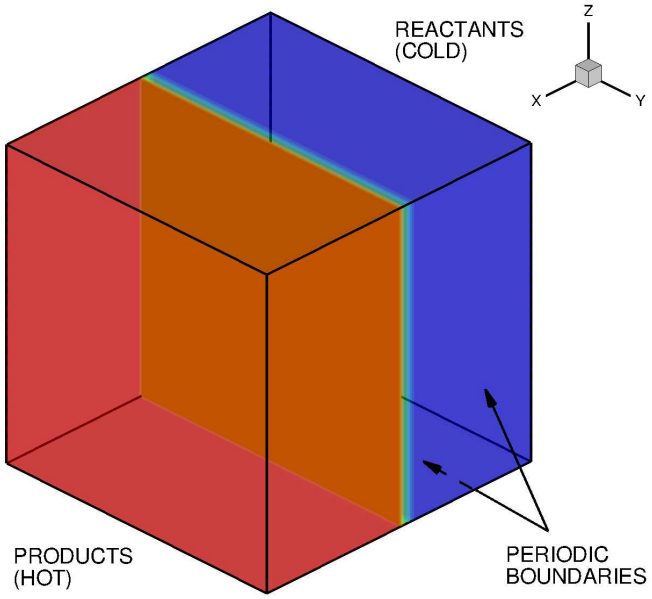

Figure 1. Configuration for the one-dimensional flame

Physical Models

The continuity, linear momentum, chemical species, and energy equations have the same form as discussed in Section 3. Nondimensional forms of the governing equations are solved. An initial turbulence spectrum is prescribed using methods outlined in (Haworth and Poinsot, 1996; Baum, 1994).

The chemistry and the radiation are coupled to the fluid dynamics (i.e., the chemical and radiative source terms feed back into the energy equation). A one-step finite-rate irreversible reaction is considered, wherein premixed reactant (R) reacts to form products (P)

$$R \rightarrow P \tag{24}$$

The Damköhler number, Da, for the reaction is 129.62. Standard molecular transport models (Newtonian viscosity, Fourier conduction, and Fickian species diffusion) are employed, where the molecular transport coefficients (viscosity μ, thermal conductivity λ, and species diffusion coefficient $\mathcal{D}$) are set such that the Prandtl number $\mathrm{Pr} = 0.75$ and Lewis number $\mathrm{Le} = 1.0$ are constant. The viscosity of the fluid is independent of the temperature. Soret and Dufour effects are not included. The working fluid is an ideal gas with constant ratio of specific heats, $\gamma = 1.4$.

Radiation properties correspond to a fictitious nonscattering gray gas with Planck-mean absorption coefficient of

$$\kappa_p = C_\kappa \left(Y_P + \epsilon_Y\right)\left[c_0 + c_1\left(\frac{A}{T}\right) + c_2\left(\frac{A}{T}\right)^2 + c_3\left(\frac{A}{T}\right)^3 + c_4\left(\frac{A}{T}\right)^4 + c_5\left(\frac{A}{T}\right)^5\right] \quad (25)$$

Coefficients A and c_0–c_5 have been taken from a radiation model (Combustion Research Facility, 2002) suggested for water vapor. Here, Y_P is the product mass fraction, ϵ_Y is an arbitrary, small, positive threshold to ensure that κ_P is nonzero everywhere, and C_κ is a coefficient that allows the optical thickness to be varied systematically and independently of other parameters. For fixed values of C_κ and Y_P, κ_P varies by more than a factor of ten over the temperature range of interest (the nondimensional $T_{\min} = 2.5$ and $T_{\max} = 10.0$ correspond to 300 and 1200 K, respectively).

Numerical Methods

Temporal integration is performed with a Runge-Kutta method of order three; for spatial discretization, a compact scheme of order six is used in the interior of the computational domain with noncentered schemes near boundaries (Poinsot and Lele, 1992). Details of the equations, normalizations, and numerical methods (in the absence of thermal radiation) can be found in (Baum, 1994).

The RTE is solved using a P_3 approximation on a $36 \times 36 \times 36$ grid. A fourth-order accurate collocation finite element method is used and the solution is obtained using direct matrix inversion (Sewell, 2005). A cubic spline is used for interpolation between the fine finite difference grid (i.e., DNS) and the coarse radiation grid.

RESULTS AND DISCUSSION

Sample Calculations for P_3 Approximation

A check on the consistency of P_3 governing equations and boundary conditions was done by considering a one dimensional medium aligned with any of the three primary global coordinates.

Next a 2D nonscattering gray medium with specified I_b and κ_P profiles was considered

$$I_b = 1 + 20r^2\left(1 - r^2\right) \quad (26)$$

$$\kappa_P = C_K\left[1 + 15\left(1 - r^2\right)^2\right] \quad (27)$$

$$r^2 = \frac{1}{2}(y^2 + z^2), \quad -1 \le y, z \le 1 \quad (28)$$

where C_K is a multiplier to change the optical thickness of the medium and it is set to unity corresponding to an optically thick medium. The walls are cold and black. The P_3 solution is compared to a photon Monte Carlo simulation (as shown in Fig. 2). It is observed that the P_3 solution matches the photon Monte carlo solution except at the

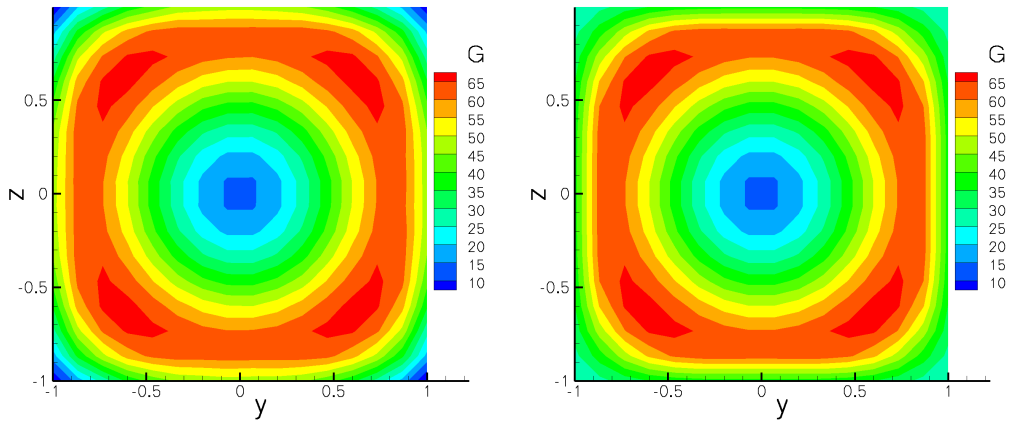

(a) Photon Monte Carlo Simulation (b) P_3 solution

Figure 2. Comparison of incident radiation, G between photon Monte Carlo simulation and P_3 approximation

boundaries. Similar comparison were made for x-y and z-x planes, and the solutions were found to be identical to the y-z plane solution.

Turbulent Premixed System

The numerical simulations are carried out using a $145 \times 144 \times 144$ computational grid. Four simulations as listed in Table 1 are carried out. An optical thickness κL based on burned-gas ($Y_P = 1.0$, $T = T_{\max} = 10.0$) properties and the initial turbulence integral length scale L characterizes thermal radiation. The turbulent Reynolds number is defined as Re$= u'_{\rm rms}L/\nu$, where $u'_{\rm rms}$ is the RMS turbulence velocity for the initial turbulent field and ν is kinematic viscosity.

Mean quantities are estimated by averaging over all grid points in the $y-z$ plane for each x location for this statistically one-dimensional configuration. The simulations proceed from the initial condition shown in Fig. 1. Premixed reactants react to form products and, due to the imposed turbulence, the flame wrinkles as shown in Fig. 3. Here t/τ is the time normalized by the initial-eddy turn over time τ, where $\tau = L/u'_{\rm rms}$. Simulations are stopped at $t/\tau = 3.57$.

Figure 3 shows the instantaneous temperature, T, isocontours for the four simulations. The temperature contours are modified slightly for the optically thin case ($\kappa_{P,2}L = 0.1$). For the optically intermediate case ($\kappa_{P,2}L = 1.0$), there is significant cooling of hot products closely behind the flame front. The optically thick case ($\kappa_{P,2}L = 10.0$) shows the largest amount of cooling of hot products, which has also altered the flame structure.

Table 1. Simulation parameters. In all cases: Da = 129.62, Pr = 0.75, Le = 1.0, and $\gamma = 1.4$

Case	Grid	$\kappa_{P,2}L$	L	Re
Case 1 (no radiation)	$145 \times 144 \times 144$	—	0.062	125
Case 2	$145 \times 144 \times 144$	0.1	0.062	125
Case 3	$145 \times 144 \times 144$	1.0	0.062	125
Case 4	$145 \times 144 \times 144$	10.0	0.062	125

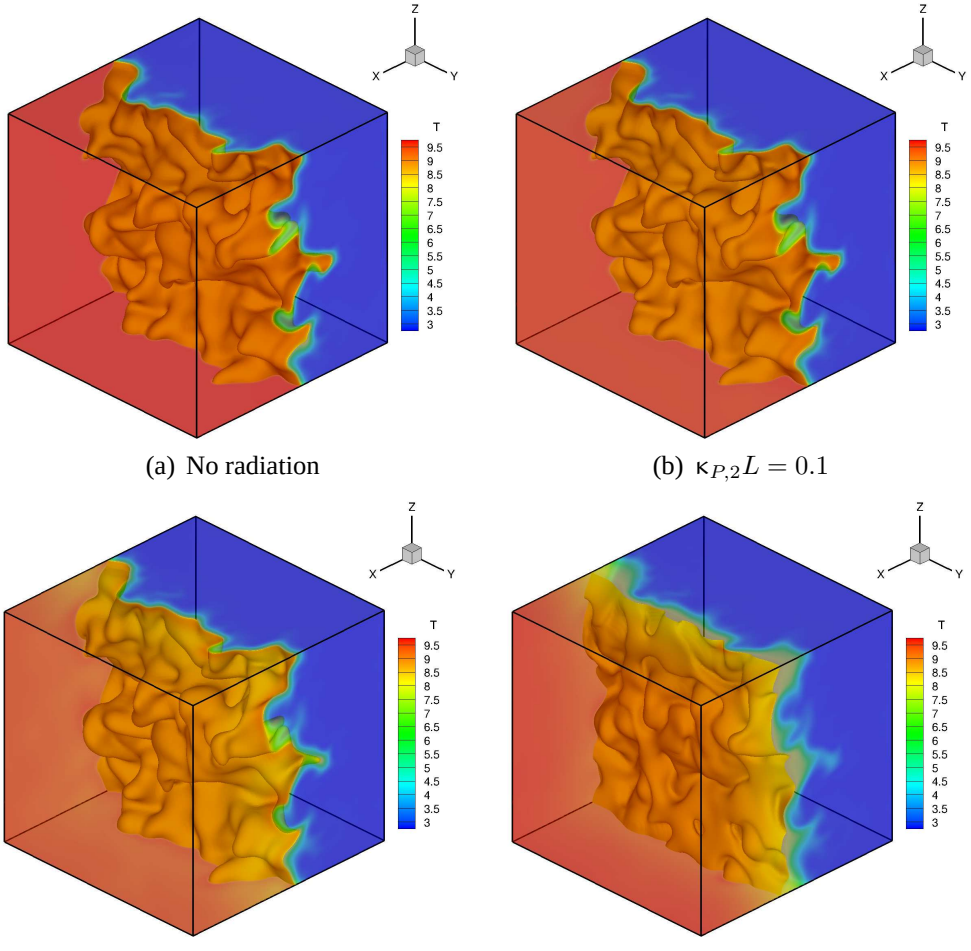

(a) No radiation (b) $\kappa_{P,2}L = 0.1$

(c) $\kappa_{P,2}L = 1.0$ (d) $\kappa_{P,2}L = 10.0$

Figure 3. Instantaneous temperature, T, isocontours without radiation and with radiation for the three values of the optical thickness at $t/\tau = 3.57$

Figure 4 shows the plane-averaged mean temperature at $t/\tau = 3.57$, the end of the simulation, along the x-direction. The mean temperature at the hot-product end of the flame front (near $x = 0.9$) decreases with increasing optical thickness. This significantly alters the gradients along the flame front and results in different cooling patterns. For the optically thick case, even though the cooling (or emission) at the flame front is maximum, away from the flame front on the hot product side most of the radiation is absorbed locally. This can be ascertained from Fig. 5. Therefore, the temperature is nearly same as for the case without radiation near the exit. For the optically intermediate case, the heat loss at the flame front is less than that for the optically thick case. But radiation travels farther in this case, and hence, the mean temperature at the exit is lower than that for the optically thick case. For the optically thin case, the heat loss at the flame front is the least but the radiation travels the farthest, which results in the lower temperature at the exit.

Emission TRI: Emission TRI quantities, discussed in Section 4, are determined for the three simulations and compared along with the no-radiation case. Figure 6 shows the temperature self-correlation factor $\mathcal{R}_{T^4}$ at $t/\tau = 3.57$ as function of normalized mean reaction progress variable $\langle Y_P \rangle$. It is unity in the pure reactants ($\langle Y_P \rangle = 0$), indicating no TRI in this region as fluctuations in this region are minimal. The correlation reaches a peak value closer to the leading edge of the flame. As seen from Fig. 6, the correlation has its largest value of about 4.8 for the no-radiation case and progressively decreases as

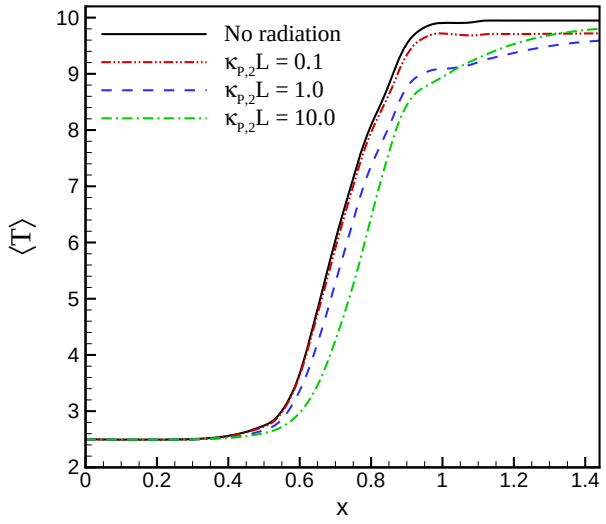

Figure 4. Mean temperature, $\langle T \rangle$, along the x-direction without radiation and with radiation for three values of the optical thickness at $t/\tau = 3.57$

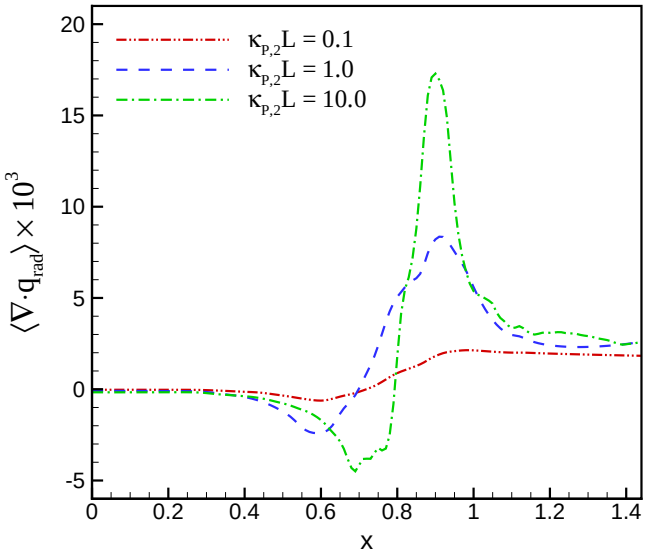

Figure 5. Mean radiative source term, $\langle \nabla \cdot q_{\mathrm{rad}} \rangle$ along the x-direction for three values of the optical thickness at $t/\tau = 3.57$

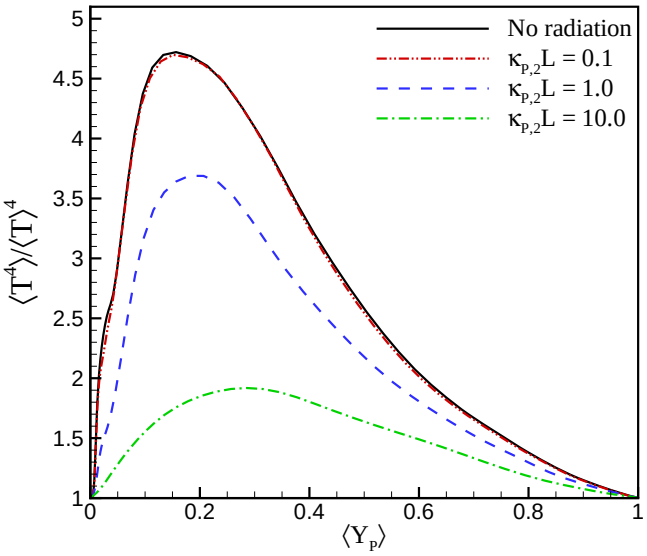

Figure 6. Temperature self-correlation $\mathcal{R}_{T^4}$, Eq. (23), versus mean progress variable $\langle Y_P \rangle$ for three values of the optical thickness at $t/\tau = 3.57$

optical thickness increases. This indicates that radiation influences the turbulent fluctuations in the medium. As emission increases with increasing optical thickness, the larger heat loss lowers the temperature and the fluctuations associated with it. The correlation falls back to unity in pure products ($\langle Y_P \rangle = 1$), indicating no TRI in this region as fluctuations in this region are minimal.

Figure 7 shows the absorption coefficient–Planck function correlation factor $\mathcal{R}_{\kappa I_b}$ at $t/\tau = 3.57$ as function of normalized mean reaction progress variable $\langle Y_P \rangle$. $\mathcal{R}_{\kappa I_b}$ is very close to zero far from the flame (where there are cold reactants or hot products), and the fluctuations are induced by the turbulence only. The trend is similar to that of the temperature self-correlation. The peak is skewed closer to the leading edge of the flame because of the combined effect of the nonlinearity of temperature and absorption coefficient fluctuations. The maximum value is reached for the no-radiation case, which same as in the temperature self-correlation.

Absorption TRI: Absorption TRI effects, shown in Fig. 8, show trends different from those of emission TRI and vary significantly with change in optical thickness, with the correlation factor decreasing with decreasing optical thickness. For the optically thick case, the profile is similar but the peak value is lower than that for emission TRI, while the absorption TRI is weak for the optically intermediate case and negligible for the optically thin case. In the optically thick case, the emitted radiation is mostly locally absorbed or travels a small distance before being absorbed. Although normally a nonlocal

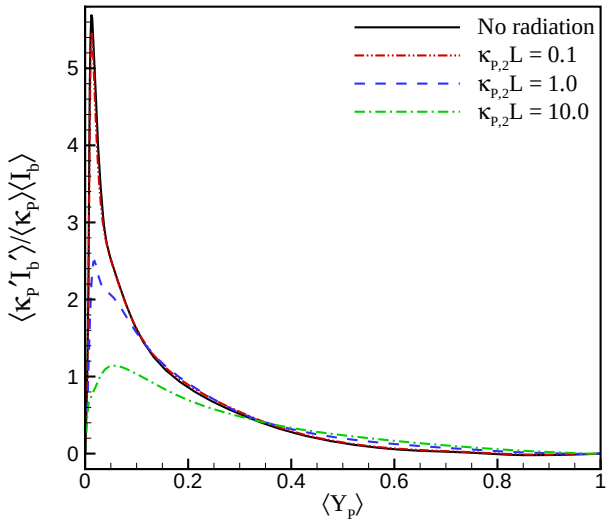

Figure 7. Absorption coefficient–Planck function correlation factor $\mathcal{R}_{\kappa I_b}$, Eq. (23), along the x-direction for three values of the optical thickness at $t/\tau = 3.57$

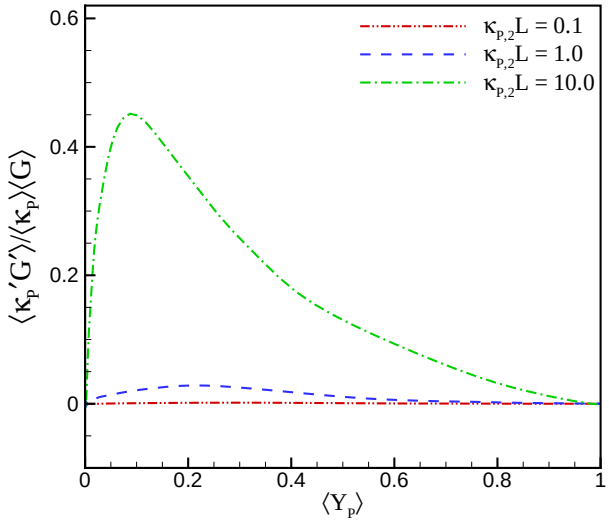

Figure 8. Absorption coefficient–intensity correlation factor $\mathcal{R}_{\kappa G}$, Eq. (23), along the x-direction for three values of optical thickness at $t/\tau = 3.57$

quantity, in an optically thick medium the incident radiation G is comprised of mostly local contributions. Hence, TRI effects for absorption are similar to those observed for emission. In the optically thin case, on the other hand, emitted radiation travels large distances with only a small fraction of it being locally absorbed. The fluctuations in the incident radiation G are thus weakly correlated with those of the absorption coefficient κ_P. Therefore, absorption TRI effects are the negligible for the optically thin case.

CONCLUSION

Direct numerical simulation coupled with a P_3 approximation has been used to explore turbulence–radiation interaction in an idealized premixed system. The temperature self-correlation, absorption coefficient–Planck function correlation, and absorption coefficient–intensity correlation have been isolated and quantified to study TRI effects.

The contributions from emission TRI (temperature self-correlation and absorption coefficient–Planck function correlation) were significant for all three optical thicknesses, while those from absorption TRI (absorption coefficient–intensity correlation) were significant for optically thick cases, weak for optically intermediate cases, and negligible for optically thin cases. For an idealized problem such as the one studied in this paper, the dynamic range of scales is small. Hence, one must exercise caution in extrapolating DNS results to practical combustion systems. DNS can, however, help in studying the influence of key dimensionless parameters (e.g., Re, Da, κL) and of the functional form of $\kappa_P(Y_P, T)$ and will ultimately help to assess and calibrate models suitable for

engineering application. In future work, DNS coupled P_3 approximation will be used to validate experimental results and provide guidance for turbulent modeling. A sensitivity study of the order of approximation (P_3, P_5, P_7, etc.) is also proposed. DNS will be also used to explore advanced scenarios involving complex chemistry, nongray-gas radiation and soot radiation.

ACKNOWLEDGMENT

The support by NASA under Grant No. NNX07AB40A is gratefully acknowledged.

REFERENCES

Baum, M. Etude de lallumage et de la structure des flammes turbulentes, Ph.D. thesis, Ecole Centrale, Paris, 1994.

Bayazitoğlu, Y. and Higenyi, J. The higher-order differential equations of radiative transfer: P3 approximation, *AIAA J.*, vol. 17, pp. 424-431, 1979.

Chai, J. C., Lee, H. S. and Patankar, S. V. Ray effect and false scattering in the discrete ordinates method, *Numer. Heat Transfer, Part B,* vol. 24, pp. 373-389, 1993.

Coelho, P. J. Detailed numerical simulation of radiative transfer in a nonluminous turbulent jet diffusion flame, *Combust. Flame*, vol. 136, pp. 481-492, 2004.

Combustion Research Facility, Sandia National Laboratories, International workshop on measurement and computation of turbulent nonpremixed flames, (http://www.ca.sandia.gov/TNF/radiation.html), 2002.

Cox, G. On radiant heat transfer from turbulent flames, *Combust. Sci. Technol.*, vol. 17, pp. 75-78, 1977.

Davison, B. Neutron Transport Theory, Oxford University Press, London, 1958.

Deshmukh, K. V., Haworth, D. C. and Modest, M. F. Direct numerical simulation of turbulence /radiation interactions in homogeneous nonpremixed combustion systems, *Proc. Combust. Inst.*, vol. 31, pp. 1641-1648, 2007.

Faeth, G. M., Gore, J. P., Chuech, S. G. and Jeng, S. M. Radiation from turbulent diffusion flames, in *Annual Review of Numerical Fluid Mechanics and Heat Transfer*, Hemisphere, Washington, DC, vol. 2, pp. 1-38, 1989.

Faeth, G. M., Jeng, S. M. and Gore, J. P. Radiation from fires, in C. K. Lau, Y. Jaluria and K. Miyasaka, Eds. *Heat Transfer in Fire and Combustion Systems*, pp. 137-151, ASME, New York, 1985.

Gore, J. P. and Faeth, G. M. Structure and spectral radiation properties of turbulent ethylene/air diffusion flames, in *Proc. of 21st Symposium (International) on Combustion*, pp. 1521-1531, 1986.

Gore, J. P. and Faeth, G. M. Structure and spectral radiation properties of luminous acetylene /air diffusion flames, *ASME J. Heat Transfer*, vol. 110, pp. 173-181, 1988.

Gore, J. P., Jeng, S. M. and Faeth, G. M. Spectral and total radiation properties of turbulent carbon monoxide/air diffusion flames, *AIAA J.*, vol. 25, pp. 339-345, 1987.

Grosshandler, W. L. and Sawyer, R. F. Radiation from a methanol furnace, ASME Paper No. 77-HT-14, 1977.

Hartick, J. W., Tacke, M., Fruchtel, G., Hassel, E. P. and Janicka, J. Interaction of turbulence and radiation in confined diffusion flames, in 26th Symposium (International) on Combustion, pp. 75-82, The Combustion Institute, Pittsburgh, 1996.

Haworth, D. C. and Poinsot, T. J. Numerical simulations of lewis number effects in turbulent premixed flames, *Combust. Flame*, vol. 104, pp. 111-137, 1996.

Kabashinikov, V. P. and Myasnikova, G. I. Thermal radiation in turbulent flowstemperature and concentration fluctuations, *Heat Transfer-Soviet Res.*, vol. 17, pp. 116-125, 1985.

Kabashnikov, V. P. Thermal radiation of turbulent flows in the case of large fluctuations of the absorption coefficient and the Planck function, *J. Eng. Phys.*, vol. 49, pp. 778-784, 1985.

Kabashnikov, V. P. and Kmit, G. I. Influence of turbulent fluctuations of thermal radiation, *J. Appl. Spectrosc.*, vol. 31, pp. 963-967, 1979.

Kabashnikov, V. P. and Myasnikova, G. I. Thermal radiation in turbulent flows-Temperature and concentration fluctuations, *Heat Transfer-Soviet Res.*, vol. 17, pp. 116-125, 1985.

Kofink, W. Complete spherical harmonics solution of the Boltzmann equation for neutron transport in homogeneous media with cylindrical geometry, *Nucl. Sci. Eng.*, vol. 6, pp. 473-486, 1959.

Kounalakis, M. E., Gore, J. P. and Faeth, G. M. Turbulence/radiation interactions in nonpremixed hydrogen/air flames, in 22nd Symposium (International) on Combustion, pp. 1281-1290, The Combustion Institute, Pittsburg, 1988.

Kounalakis, M. E., Gore, J. P. and Faeth, G. M. Mean and fluctuating radiation properties of nonpremixed turbulent carbon monoxide/air flames, *ASME J. Heat Transfer*, vol. 111, pp. 1021-1030, 1989.

Kounalakis, M. E., Sivathanu, Y. R. and Faeth, G. M. Infrared radiation statistics of nonluminous turbulent diffusion flames, in *Proc. of 3rd ASME/JSME Thermal Engineering Joint Conference*, vol. 5, pp. 3-12, ASME, New York, 1991.

Krebs, W., Koch, R., Eigenmann, L. and Wittig, S. Effect of temperature and concentration fluctuations on radiative heat transfer in turbulent flames, in 26th Symposium (International) on Combustion, pp. 2763-2770, The Combustion Institute, Pittsburgh, 1996.

Kritzstein, F. and Soufiani, A. Infrared gas radiation from a homogeneously turbulent medium, *Int. J. Heat Mass Transfer*, vol. 36, pp. 1749-1762, 1993.

Li, G. and Modest, M. F. Investigation of turbulenceradiation interactions in reacting flows using a hybrid FV/PDF Monte Carlo method, *J. Quant. Spectrosc. Radiat.*

Transfer, vol. 73, pp. 461-472, 2002.

Li, G. and Modest, M. F. Importance of turbulenceradiation interactions in turbulent diffusion jet flames, *ASME J. Heat Transfer*, vol. 125, pp. 831-838, 2003.

Marshak, R. E. Note on the spherical harmonics method as applied to the Milne problem for a sphere, *Phys. Rev.*, vol. 71, pp. 443-446, 1947.

Mazumder, S. and Modest, M. F. A PDF approach to modeling turbulenceradiation interactions in nonluminous flames, International, *J. Heat Mass Transfer*, vol. 42, pp. 971-991, 1999a.

Mazumder, S. and Modest, M. F. Turbulenceradiation interactions in nonreactive flow of combustion gases, *ASME J. Heat Transfer*, vol. 121, pp. 726-729, 1999b.

Mengüç, M. P. and Viskanta, R. Radiative transfer in three-dimensional rectangular enclosures containing inhomogeneous, anisotropically scattering media, *J. Quant. Spectrosc. Radiat. Transfer*, vol. 33, pp. 533-549, 1985.

Modest, M. F. The modified differential approximation for radiative transfer in general threedimensional media, *J. Thermophys. Heat Transfer*, vol. 3, pp. 283-288, 1989.

Modest, M. F. Radiative Heat Transfer, 2nd Ed., Academic Press, New York, 2003.

Nelson, D. A. Band radiation from a fluctuating medium, *ASME J. Heat Transfer*, vol. 111, pp. 131-134, 1989.

Olfe, D. B. A modification of the differential approximation for radiative transfer, *AIAA J.*, vol. 5, pp. 638-643, 1967.

Ou, S. C. S. and Liou, K. N. Generalization of the spherical harmonic method to radiative transfer in multi-dimensional space, *J. Quant. Spectrosc. Radiat. Transfer*, vol. 28, pp. 271-288, 1982.

Poinsot, T. and Lele, S. Boundary conditions for direct numerical simulations of compressible viscous flows, *J. Comput. Phys.*, vol. 101, pp. 104-129, 1992.

Ratzel, A. C. and Howell, J. R. Two-dimensional radiation in absorbingemittingscattering media using the P-N approximation, *ASME J. Heat Transfer*, vol. 105, pp. 333-340, 1983.

Sewell, G. The Numerical Solution of Ordinary and Partial Differential Equations, 2nd Ed., Wiley, Hoboken, NJ, 2005.

Song, T. H. and Viskanta, R. Interaction of radiation with turbulence: Application to a combustion system, *J. Thermophys. Heat Transfer*, vol. 1, pp. 56-62, 1987.

Soufiani, A., Mignon, P. and Taine, J. Radiationturbulence interaction in channel flows of infrared active gases, in *Proc. of 9th International Heat Transfer Conference*, Hemisphere, vol. 6, pp. 403-408, Washington, DC, 1990a.

Soufiani, A., Mignon, P. and Taine, J. Radiation effects on turbulent heat transfer in channel flows of infrared active gases, in *Proc. of 1990 AIAA/ASME Thermophysics and Heat Transfer Conference*, vol. HTD-137, pp. 141-148, ASME, New York, 1990b.

Souil, J. M., Joulain, P. and Gengembre, E. Experimental and theoretical study of ther-

mal radiation from turbulent diffusion flames to vertical target surfaces, *Combustion Science and Technol.*, vol. 41, pp. 69-81, 1984.

Tamanini, F. Reaction rates, air entraiment and radiation in turbulent fire plumes, *Combust. Flame*, vol. 30, pp. 85-101, 1977.

Tessè, L., Dupoirieux, F. and Taine, J. Monte Carlo modeling of radiative transfer in a turbulent sooty flame, *Int. J. Heat Mass Transfer*, vol. 47, pp. 555-572, 2004.

Tong, T. W. and Swathi, P. S. Radiative heat transfer in emittingabsorbingscattering spherical media, *J. Thermophys. Heat Transfer*, vol. 1, pp. 162-170, 1987.

Viskanta, R. and Mengüç, M. P. Radiation heat transfer in combustion systems, *Prog. Energy Combust. Sci.*, vol. 13, pp. 97-160, 1987.

Wilcox, D. C. Model for fires with low initial momentum and nongray thermal radiation, *AIAA J.*, vol. 13, pp. 381-386, 1975.

Wu, Y., Haworth, D. C., Modest, M. F. and Cuenot, B. Direct numerical simulation of turbulence /radiation interaction in premixed combustion systems, *Proc. Combust. Inst.*, vol. 30, pp. 639-646, 2005.

Wu, Y., Modest, M. F. and Haworth, D. C. A high-order photon monte carlo method for radiative transfer in direct numerical simulation, *J. Comput. Phys.*, vol. 223, pp. 898-922, 2007.

Yang, J. and Modest, M. F. High-order P-N approximation for radiative transfer in arbitrary geometries, *J. Quant. Spectrosc. Radiat. Transfer*, vol. 104, pp. 217-227, 2007.